Journal Pre-proof

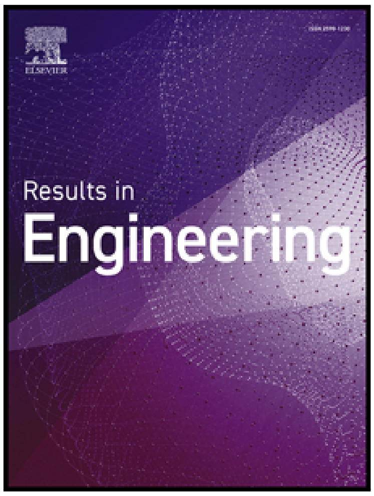

Modeling the Influence of Grip and Push Force Variations on the Mechanical Impedance and Vibration Power Absorption of the Hand-Arm System

Carina Spengler, Simon Saurbier, Andreas Lindenmann, Markus Doellken, Lukas Bunk, Dieter Krause, Sven Matthiesen

PII: S2590-1230(26)04162-9
DOI: https://doi.org/10.1016/j.rineng.2026.113151
Reference: RINENG 113151

To appear in: *Results in Engineering*

Received date: 13 August 2025
Revised date: 22 July 2026
Accepted date: 21 September 2026

Please cite this article as: Carina Spengler, Simon Saurbier, Andreas Lindenmann, Markus Doellken, Lukas Bunk, Dieter Krause, Sven Matthiesen, Modeling the Influence of Grip and Push Force Variations on the Mechanical Impedance and Vibration Power Absorption of the Hand-Arm System, *Results in Engineering* (2025), doi: https://doi.org/10.1016/j.rineng.2026.113151

Highlights

Modeling the Influence of Grip and Push Force Variations on the Mechanical Impedance and Vibration Power Absorption of the Hand-Arm System

Carina Spengler,Simon Saurbier,Andreas Lindenmann,Markus Doellken,Lukas Bunk,Dieter Krause,Sven Matthiesen

- Experimental measurements conducted at 10×10 combinations of grip and push forces
- Mechanical impedance (MI) increased up to 3x for grip and 2x for push-force changes
- Grip force has stronger influence on vibration power absorption (VPA) than push force
- MI and VPA at intermediate forces can be reliably predicted via linear interpolation
- With 3 levels of grip and push force, prediction accuracy of MI and VPA is $\geq$ 95 %

Modeling the Influence of Grip and Push Force Variations on the Mechanical Impedance and Vibration Power Absorption of the Hand-Arm System

Carina Spengler[a,1], Simon Saurbier[a,*,1], Andreas Lindenmann[a], Markus Doellken[a], Lukas Bunk[b], Dieter Krause[b] and Sven Matthiesen[a]

[a] *Karlsruhe Institute of Technology (KIT), IPEK - Institute of Product Engineering, Kaiserstrasse 10, Karlsruhe, 76131, Germany*
[b] *Hamburg University of Technology, PKT - Institute of Product Development and Mechanical Engineering Design, Denickestraße 17 (L), Hamburg, 21073, Germany*

ARTICLE INFO

Keywords:
hand-arm vibration
vibration behavior
modeling
coupling forces
human-machine interaction
power tools
occupational health

ABSTRACT

Understanding the vibration behavior of the hand-arm system (HAS) is essential for product development and occupational health. Although push and grip forces strongly influence HAS vibrations, the appropriate approach for modeling force-dependent mechanical impedance (MI) and vibration power absorption (VPA) remains unclear. This study systematically examines MI and VPA along the z_h-axis for translational excitation in five subjects using 1,500 measurements across a 10×10 grid of push and grip force combinations, covering push forces of 10–110 N and grip forces of 10–135 N. Unlike previous studies with only few discrete force combinations, this high-resolution force grid not only enables a detailed characterization of force-dependent behavior, but also, for the first time, the systematic evaluation of interpolation-based prediction across the force domain. The results show that grip force dominates MI in the 30–70 Hz and 160–500 Hz ranges, while push force has the greatest influence between 50 Hz and 110 Hz. Higher forces generally increase VPA, but reduce it in the low-frequency range of 10–30 Hz. Compared with ISO 10068:2012, measured MI values deviate from the standardized range, especially at higher grip and push forces, reaching up to four times higher values and thereby also affecting VPA as a derived quantity. Linear interpolation using only three discrete force levels predicts MI and VPA at intermediate force levels with at least 95 % mean accuracy based on MAPE. These findings show that force-dependent HAS responses can be represented with substantially reduced experimental effort, providing a basis for physical and simulation-based models with continuously variable coupling forces.

1. Introduction

Applications involving manually operated technical systems often expose the hand-arm system (HAS) to vibration, particularly when hand-held tools are used. In these applications, the hand forms the main interface between the user and the tool. The practical relevance of this research is illustrated by applications such as hammer drilling [31] or nail gun operation [44], where users can be exposed to high vibration levels. The forces generated by hand-held tools are transmitted to the user through the handle and act on the HAS as dynamic loads. Repeated hand-arm vibration exposure can lead to health problems such as white finger syndrome [38]. This occupational health relevance is reflected in ISO 5349-1:2001, which addresses vascular, neurological, and musculoskeletal effects of hand-arm vibration exposure [25]. This standard provides a basis for assessing and comparing hand-arm vibration exposure. Recent research therefore emphasizes the need to consider vibration effects already during the development of hand-held devices [37].

The resulting vibration behavior depends not only on the tool but also on the biodynamic properties of the HAS, such as mass, stiffness, and damping. The specific challenge of hand-held tools is that the interaction with the user can alter the operating parameters, including tool vibrations; therefore, user-related parameters such as grip force, push force, posture, and anthropometry have to be considered in product configuration and vibration analysis [30, 28, 35, 43, 11]. For product development, it is necessary to understand how coupling forces affect the

*Corresponding author
carina.spengler@kit.edu (C. Spengler); simon.saurbier@kit.edu (S. Saurbier)
ORCID(s): 0009-0002-1762-0946 (C. Spengler); 0009-0000-5679-7977 (S. Saurbier)
[1] Shared first authors

biodynamic response of the HAS during the use of hand-held tools. Based on such data, physical and simulative models of the HAS can be developed. These enable the vibration exposure and behavior of the operating parameters to be analyzed with changing push and grip forces as well as other factors. With knowledge about the vibration transmission the products can be adjusted at an early stage in the development process. To describe the dynamic vibration behavior the mechanical impedance (MI) and the vibration power absorption (VPA) can be used. The MI is a biodynamic response function and describes the relationship between the dynamic force and the vibration velocity input to the HAS [42, 26]. In product development, MI can be used as a boundary condition in vibration analyses and as a user-dependent biodynamic parameter [30, 35]. The VPA describes the absorbed power into the HAS and is derived from the real part of the MI and the vibration acceleration input to the HAS [26]. Previous studies have shown that the MI and VPA are influenced by different factors, like grip force, push force, vibration dose, handle size, posture and anthropometric data [30, 4, 3, 7, 9]. It is known that a variation in the grip and push forces causes changes in the stiffness and damping properties as well as the effective mass of the HAS and the coupling between the hand and the measuring handle [39, 18, 45, 17]. ISO 10068:2012 specifies a value range for grip forces of 25–50 N and for push forces of less than 50 N in three orthogonal directions [26]. Lindenmann et al. already noted in 2021 that these interaction forces do not necessarily correspond to real-world applications [31]. For this reason, they conducted a study to determine the grip and push forces that occur when using a power tool. The study showed a large effect of grip force, a medium to large effect of push force, and a weak effect of posture on MI. However, previous studies on MI and VPA of the HAS are limited in at least one of the following aspects: They investigated either only low force levels, only grip or push force, or only two to three discrete force combinations, e.g. [39, 4, 3, 6, 30]. This does not provide knowledge about the behavior of the MI and VPA between these forces, even though a continuous spectrum of grip and push forces occurs when using hand-held tools. This reflects a broader limitation in previous studies on the MI and VPA of the HAS often include only a small number of subjects, usually four to eight, and a limited number of force combinations due to the long duration of the experiments [22, 23, 5, 29, 36]. The objective of this work is therefore to investigate whether the force-dependent behavior of MI and VPA can be predicted for intermediate push or grip force levels within an extended force range. In contrast to previous studies with only a few discrete force combinations, this study uses MI and VPA measurements collected on a systematic 10×10 grid of grip and push forces to analyze the influence of both forces and to evaluate whether linear interpolation between measured force levels is sufficient for reliable prediction. This is performed both on an individual level, using subject-specific data, and on an aggregated level, using pooled data across all subjects. The resulting force-dependent MI and VPA curves are additionally examined to characterize the functional behavior between minimum and maximum force levels, for example whether the trends are approximately linear or show stronger nonlinear characteristics. This approach could reduce the workload for subjects in future studies while preserving the main force-dependent characteristics of MI and VPA.

From this objective the following research questions can be derived:

RQ1: How do different push and grip forces influence the mechanical impedance and vibration power absorption along the translational z_h-axis of the hand-arm system?

RQ2: How many discrete levels of push or grip force are required to predict the mechanical impedance and vibration power absorption at intermediate force levels within the investigated force range with an accuracy of at least 95 %?

2. Materials and methods

2.1. Experimental Design

The data of this study was recorded with five subjects on a test rig for generating axial and angular vibrations [34]. The test rig consists of two electromechanical shakers. An axial shaker ($M124M$, ETS Solutions Europe GmbH, Loffenau, Germany) and a rotational shaker ($L215M$, ETS Solutions Europe GmbH, Loffenau, Germany). In this test setup, the user interaction test rig is used to measure the excitation force and the acceleration at the point of excitation while the subjects HAS was excited translationally along the z_h-axis of the human-centered coordinate system defined in the ISO 5349-1:2001 [25]. The axial shaker is operated in a frequency range from 10 Hz to 500 Hz using a multisine signal, according to [30]. In addition, the upper limit was chosen based on the ISO 10068:2012 [26]. The frequency gradation was adopted from the state of research by Griffin [21]. The measuring handle in accordance with the german institute for standardization (DIN) standard DIN EN ISO 10819:2022 [14] is attached to the end effector of the shaker (see Figure 1). The cylindrical measuring handle is equipped with two one-axial force sensors (Type 9011A, Kistler

Table 1
Anthropometric data of the subjects, measurements performed according to ISO 7250 [27].

Anthropometric Data	Subject 1	Subject 2	Subject 3	Subject 4	Subject 5
Body weight in kg	95	66	82	93	67
Hand weight in kg	0.52	0.33	0.42	0.50	0.28
Body height in cm	186	166	181	196	168
Arm length in cm	86.3	63.0	70.5	91.2	69.5
Forearm length in cm	29.0	24.5	28.5	30.0	27.5
Hand length in cm	20.0	17.5	18.8	18.8	16.5
Palm length in cm	11.1	9.5	10.2	11.5	9.0
Palm width in cm	10.0	8.0	8.8	9.5	7.3
Thumb length in cm	7.0	5.8	6.5	6.6	5.8

Table 2
Factor levels of push force and grip force used in the experimental study.

	Factor levels									
Push force in N	10	21	32	43	54	65	76	87	98	110
Grip force in N	10	24	38	52	66	80	94	108	122	135

Instrumente AG, Winterthur, Switzerland) and two three-axial force sensors (Type 9027C, Kistler Instrumente AG, Winterthur, Switzerland). Furthermore, two accelerometers (Type 356A15, PCB Piezotronics GmbH, Hueckelhoven, Germany) are attached to the measuring handle. The measurement signals were recorded using the ADwin Pro II measurement system (Jaeger Computergesteuerte Messtechnik GmbH, Lorsch, Germany). The measuring handle was calibrated according to the method developed by Heyden et al. in the frequency range from 10 Hz to 500 Hz [24]. The recorded measurements are published in [12].

2.2. Experimental Procedure

Ethical approval was granted by the Ethics Committee of (no. A2025-018). All subjects provided written informed consent. They were informed about the procedures as well as data handling and could withdraw consent and discontinue participation at any time. Prior to the measurements, anthropometric data of the subjects were acquired in accordance with ISO 7250-1:2017 [27]. The study director was instructed to ensure that the anthropometric measurements remained consistent across the subjects, for example that hand width was always measured at the widest point. The hand weight was measured by placing the hand in a water-filled box and determining the additional weight. The data is listed in Table 1. Subjects 1, 3 and 4 are male, while subjects 2 and 5 are female. The subjects are aged between 23 and 34 years, with an average age of 27.5 years.

The height of the axial shaker was adjusted so that the subject's elbow was at an angle of approximately 90 °. The wrist was kept neutral. The foot position was also defined and predetermined with a shoulder-width offset stance. This ensured that the posture of all subjects was identical. The posture in the measurement acquisition is in the range of ISO 10068:2012 [26]. The lowest factor level of the push and grip forces to be investigated were derived from the current state of research. The upper factor level corresponds to the applied forces by professional users in a hammer drill study by Lindenmann et al. [31]. The gradations of the factor levels in Table 2 were determined mathematically. The definitions of push and grip forces are in accordance with DIN 45679:2013-2 [13].

The study was conducted in a full factorial experimental plan with three repetitions per combination. The order of the measurements was randomized. In total 300 measurements per subject were performed. To prevent fatigue, the measurements were carried out on different days, with four to seven sessions per subject. On average, there were 12 days between the sessions for each subject. Depending on the physical condition of the subject, between one and 100 measurements were recorded in each session. The series of measurements was interrupted after every 10 measurements, with additional breaks taken depending on the subject. During each measurement, the measured push and grip forces were visualized together with the target forces from the experimental plan graphically in real time. The graphical user interface enables the subject to set the target push and grip forces before the start of the recording and to compare and, if necessary, adjust it during the measurement. The excitation was carried out with a multisine to minimize the

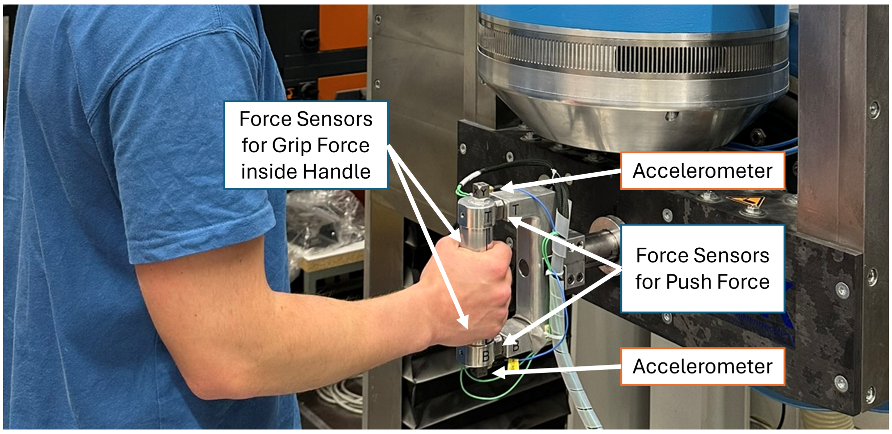

Figure 1: Study set-up on the test rig: The subject's posture is according to the defined ranges in ISO 10068:2012 [26]. The measuring handle is built up according to DIN EN ISO 10819:2022 [14]. The handle is equipped with two one-axial force sensors for measuring the grip force, two three-axial force sensors for measuring the push force and two accelerometers.

exposure time to 16.5 sec for each measurement. The multisine signal is composed with several sine waves between 10 to 500 Hz with a 5 Hz increment, as described in [30]. The unweighted root-mean-square acceleration of the multisine excitation was 30 m/s^2. For subject 1, the applied RMS acceleration was approximately 1.1 times higher than for the remaining subjects. The measured value of the total vibration value (a_{hv}) according to ISO 5349-1:2001 was 6.5 m/s^2, which results in a vibration dose of 0.594 m/s^2 [25]. This value is below the upper limit value of 5 m/s^2 and the trigger value for the vibration-reducing measures of 2.5 m/s^2. Therefore, the risk to the subjects can be classified as low.

2.3. Data Analysis

The measured data is evaluated in MATLAB (The Math Works Inc., Natick, USA). The 1500 recorded measurements, 300 measurements per subject ($n = 5$), were shortened to 11 sec each to ensure that the software ramp-up and ramp-down is not taken into account in the subsequent data processing steps. Shortened data sets were excluded if the deviation of the push and grip forces from the target forces exceeded ± 5 N or 14 %. These absolute and percentage limits were chosen to allow for similar deviations in grip and push forces at high and low levels without excluding a substantial amount of data. The higher of the two limits (5 N or 14 %) was always used for exclusion. For the remaining measurements, the MI was calculated according to formula 1 and the VPA was calculated separately using formula 2. The evaluation of the multisine signal is conducted according to Lindenmann et al. [30].

Mechanical impedance (MI) is defined as the complex-valued ratio of force to velocity at the point of force application within the frequency domain. MI characterizes a system's dynamic mechanical behavior as a function of angular frequency, ω in rad/s. MI is expressed as follows:

$$MI(\omega) = \frac{F(\omega)}{v(\omega)} = \Re(MI(\omega)) + i * \Im(MI(\omega)) \quad (1)$$

Here, $F(\omega)$ denotes the force spectrum in N, and $v(\omega)$ denotes the velocity spectrum in meters per second (m/s). Thus, the unit of MI is Ns/m. MI can be decomposed into real and imaginary components. The real part represents the energy dissipated in the hand-arm system per time unit, and the imaginary part corresponds to reversible energy storage without net power dissipation [16].

The VPA is defined as the product of the frequency-dependent force and velocity at the point of force application, representing the mechanical power absorbed by the system [16]. In the frequency domain, VPA can be expressed as

$$VPA(\omega) = \Re(MI(\omega)) * |v(\omega)|^2 \quad (2)$$

with $\Re(MI(\omega))$ being the real part of the mechanical impedance in Ns/m, and $|v(\omega)|^2$ being the squared absolute velocity in m^2/s^2. Consequently, the resulting VPA has the unit W. Only the real part of the mechanical impedance contributes to absorbed mechanical power.

Table 3
Combinations of grip and push force curves for two, three or four grid curves.

Two grid curves		Three grid curves		Four grid curves	
Push force in N	Grip force in N	Push force in N	Grip force in N	Push force in N	Grip force in N
21	24	21	24	21	24
110	135	65	80	54	66
-	-	110	135	76	94
-	-	-	-	110	135

To be able to compare and visualize possible effects all measurement combinations are clustered. The median of the magnitude of MI and VPA are calculated for all measurements in which the grip force was constant and the push force varied and vice versa. For example, the 10 N grip force curve consists of the median of the 10 push force levels from 10 to 110 N with three repetitions each. This results in 10 MI and VPA vectors for grip force and 10 for push force. Thus, each curve represents the influence of either push or grip force, while the influence of the other force is aggregated across its measured range. This procedure was applied for the individual subjects as well as the aggregated data set including all subjects. Each of the curves created for one of the subjects consists of 30 measurements, and each median curve for the aggregated data set of subjects consists of 150 measurements. The absolute values of the curves were used to create the diagrams.

A linear approach is chosen to model the influence of push and grip forces on the MI and the VPA separately. For the interpolation, the 10 median curves per subject for push and grip forces are used as well as the combination of all subjects. Since the 10 N push and grip forces often led to an exclusion as described above, the next lowest factor level of the push and grip forces is defined as the lower curve for the interpolation. The upper curve for interpolation is the highest factor level of the respective force (110 or 135 N). The curves used for interpolation are referenced as grid curves in the following. Depending on the number of grid curves, the mean curve or two curves with as even a distribution as possible between the peripheral curves are added (see Table 3). The curves are also clustered for interpolation as described in the previous paragraph. The absolute values of the grid curves are used. The interpolation was carried out between the next lowest and next highest grid curve, depending on the distance in percent. This is carried out for push and grip force combinations that are not used as grid curves.

The validation of the determined interpolation curves is carried out for all push and grip force levels that are not used as grid curves. The deviation of the interpolated curve from the real measurement is evaluated using the following error metrics. RMSE averages the error with sensitivity to large deviations, RRMSE normalizes it as a percentage and MAPE provides a relative error measure that is less sensitive to outliers.

- Root mean squared error (RMSE) quantifies the average magnitude of deviation between predicted and true values. It is expressed in the same physical unit as the measured data,

$$RMSE = \sqrt{\frac{1}{n} * \sum_{i=1}^{n} (y_{true,i} - y_{pred,i})^2} \tag{3}$$

  where $y_{true,i}$ denotes the i-th reference (true) value and y_{pred} the corresponding predicted value. The variable n represents the total number of samples.

- The relative root mean squared error (RRMSE) is a normalized error metric expressed as a percentage that allows for comparison across data sets with different magnitudes. It is obtained by normalizing the RMSE with respect to the mean of the reference values and is given by:

$$RRMSE = \frac{RMSE}{mean(y_{true})} * 100 = \frac{\sqrt{\frac{1}{n} * \sum_{i=1}^{n} (y_{true,i} - y_{pred,i})^2}}{mean(y_{true})} * 100 \tag{4}$$

  where the mean of the reference values is denoted by mean y_{true}.

- The mean absolute percentage error (MAPE) expresses the average relative deviation between the predicted and true values as a percentage. It is defined as:

$$MAPE = \frac{1}{n} * \sum_{i=1}^{n} |\frac{(y_{true,i} - y_{pred,i})}{y_{true,i}}| * 100 \quad (5)$$

The absolute value ensures that positive and negative deviations contribute equally to the error metric.

3. Results

In total 150 of 1500 measurements exceeded the permissible tolerance (see Section 2.3) from the specified force in the measurement recordings and were therefore excluded from further data processing. The standard deviation of the three measurement repetitions for the magnitude of MI across all subjects is between 3.4 and 59.5 Ns/m with a mean standard deviation of 20.5 Ns/m. The mean magnitude of MI value is 254.9 Ns/m. The standard deviation for the VPA is between 0.0021 and 0.047 W, with the mean standard deviation of the VPA across all measurements being 0.013 W. The mean VPA value is 0.024 W. Given the large number of possible figures, the following results are presented for the magnitude of MI; the observed trends were also found for the phase angle of MI. The figures show clustered and aggregated values from subjects 1–5, while the same trends were also observed in the individual subject curves. The dataset obtained from the data acquisition is available in [12] and provides the magnitude and phase angle of MI and VPA for each subject, force combination, and measurement repetition. The mean error metrics for the prediction of magnitude of MI and VPA of each subject and the aggregated subjects are given in tables in this section, the error metrics of each force combination can be found in the Appendix A.

3.1. RQ1: How do different push and grip forces influence the mechanical impedance and vibration power absorption along the translational z_h-axis of the hand-arm system?

To answer RQ1 the results are divided into three subsections. First, the broadening caused by force variation is analyzed for both the magnitude of MI and VPA, including inter-subject variability. Afterwards, the influence of the push and grip forces on the magnitude of MI and the VPA are described separately.

3.1.1. Distribution due to grip and push force variation and inter-subject variability

Figure 2 shows the magnitude of the MI of all measurements per subject over the frequency range. The solid curve represents the median values for each subject, while the shaded area represents the range between the 5th and 95th percentile. Focusing on the solid curves, it can be seen that the median magnitude of MI varies for each subject. The influence between the subjects results in median MI magnitude values between 100 and 430 Ns/m over the frequency range. Subjects 1, 3 and 4 have a global maximum between 30 and 35 Hz, followed by a local minimum between 60 and 70 Hz, a local maximum at about 100 Hz, a local minimum of around 115-130 Hz and a progression with a linear gradient afterward until 500 Hz. In contrast, subjects 2 and 5 have their global maximum at 40 Hz and miss the local minimum around 60-70 Hz. The remainder follows the progression described above. Compared with the other subjects, subjects 2 and 5 show lower MI magnitude values at frequencies above 100 Hz, while subject 5 also exhibits a lower global maximum. Subjects 2 and 5 are female, while the other three are male. Taking into account the 5th and 95th percentile of the measurements, the median values per subject expand into broader ranges, as shown by the shaded areas. In contrast to the solid curves, these areas consider grip and push forces between 10 and 110 N and between 10 and 135 N. The upper contours of the shaded areas shift to higher frequencies for MI magnitude values above the median, while the lower contours shift to lower frequencies for MI magnitude values below the median. The contribution of grip and push forces results in a broadening of the median MI magnitude curves to values between 50 and 950 Ns/m across all frequencies for the 5th to 95th percentile of the measurements. For subject 3 the magnitude of MI has its highest broadening with an increase by 15.8 times at 50 Hz.

Figure 3 displays the VPA over the frequency range per subject. The solid curves represent the median VPA of all measurements of each subject, while the shaded area includes the 5th to 95th percentile of the measurements. The median VPA values for all subjects (solid curves) vary between $8*10^{-4}$ and 0.38 W over the frequency range. The median VPA curves vary for each subject. Subject 1, in particular, reaches higher VPA values between 10 to 35 Hz compared to the remaining subjects. Starting with values between 0.09 and 0.21 W the progressions follow a linear gradient, which merges into the global maximum between 30 and 35 Hz. Afterwards, the curves decrease strongly till

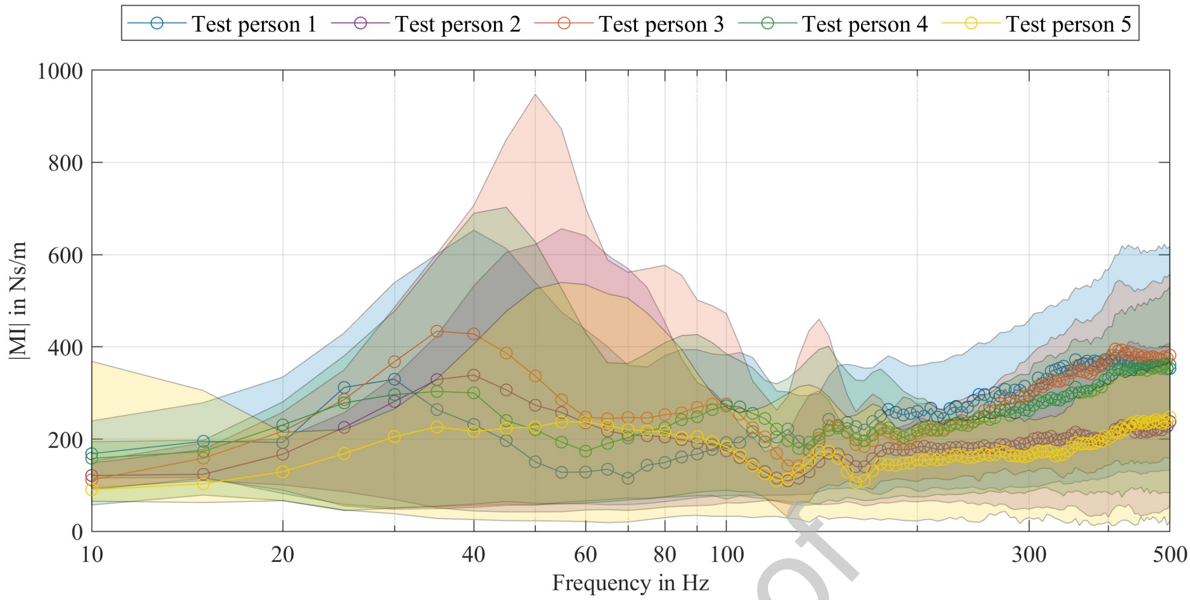

Figure 2: The magnitude of mechanical impedance over the frequency range. The graph consists of 300 measurements for each subject. The median values are displayed as solid curves and the shaded areas cover the 5th to 95th percentile. In contrast to the solid curves, the shaded areas take into account the measurements of the range of push and grip forces from 10 to 110 N, respectively from 10 to 135 N.

60 Hz and are approaching zero for higher frequencies. Observing the 5th to 95th percentile of each subject, it can be seen that the progression follows the median values, but the range gets wider. The values of the shaded area above all frequencies are between $3.5*10^{-5}$ and 0.59 W. The shaded area, which takes grip and push forces into account, has a wider VPA value range than the median curves.
These inter-subject differences may be related to anthropometric characteristics. Both the inter-subject differences and the grip and push force combinations influence the magnitude of MI and VPA.

3.1.2. *Influence of push and grip forces on the MI*

The magnitude of MI is shown for varying push forces in Figure 4 between 10 to 110 N and varying grip forces in Figure 5 between 10 to 135 N over the frequency range from 10 to 500 Hz. The measurements are merged according to Section 2.3 *Clustering of Measurements*. Additionally, the magnitude of MI range of ISO 10068:2012 is displayed in the Figures 4 and 5 [26]. The conducted measurements of all subjects are shown and described here as an example; the same general trends were also observed for each individual subject. The solid curves represent the median value of the push and grip force levels, while the shaded areas represent the 5th to 95th percentile of the respective push or grip force level, illustrating the variation in the measurements. The color gradient in the Figure is used to differentiate between force levels: lower force levels are represented in green, while higher force levels fade to shades of orange for recognition of trends across different forces.

In Figures 4 and 5 it can be seen that the magnitude of MI curve of the lowest push or grip force of 10 N has the lowest values for each frequency. The higher the push or grip force level gets, the more the MI magnitude values increase. Furthermore, it can be seen, that the minima and maxima shift to higher frequencies for increasing push and grip forces. The distance between the MI magnitude curves for each force level of push and grip forces are almost linear for each frequency. A gap occurs between the grip force levels of 66 and 80 N in the frequency range from 30 to 70 Hz, representing the only range in which an approximately linear increase is not observed, see Figure 5. The influence of the different push forces on the magnitude of MI is predominantely for frequencies between 50 and 110 Hz, see Figure 4. For varying grip forces the influence on the magnitude of MI is prevalent for frequencies between 30-70 Hz and 160-500 Hz. Comparing the effects of push and grip force on the magnitude of MI, it can be seen that grip forces already have an influence at lower frequencies than push forces. The MI magnitude curves for different grip forces in Figure 5 are diverging already from 10 Hz on. The influence of push forces on the magnitude of MI is highest at 55 Hz

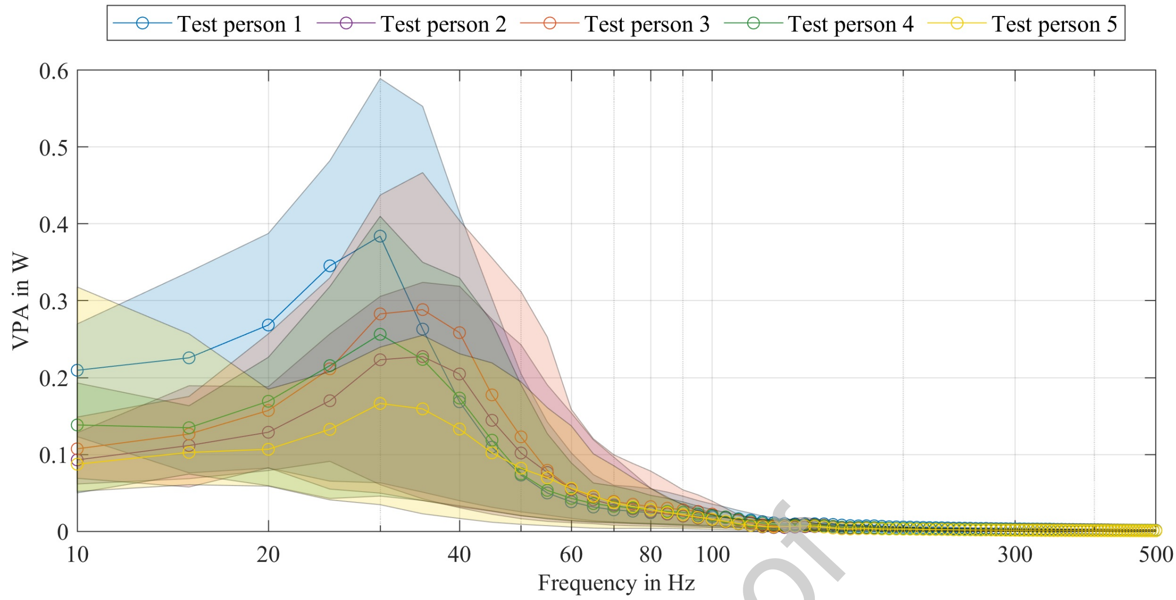

Figure 3: The vibration power absorption over the frequency range. The graph consists of 300 measurements for each subject. The median values are displayed as solid curves and the shaded areas cover the 5th to 95th percentile. In contrast to the solid curves, the shaded areas take into account the measurements of the range of push and grip forces from 10 to 110 N, respectively from 10 to 135 N.

with a difference of 177 Ns/m, see Figure 4. At 40 Hz the influence of the grip force on the magnitude of MI reaches a maximum difference of 318 Ns/m, see Figure 5. Above 160 Hz the influence of the push force on the magnitude of MI is small. In contrast, the grip force strongly influences the frequencies above 160 Hz and becomes progressively larger with increasing frequency. The difference of the MI magnitude values at 500 Hz is 290.2 Ns/m, only marginally below the maximum difference at 40 Hz. The second maximum at approx. 85 Hz is particularly pronounced for varying push forces, whereas it is not as high for varying grip forces. Overall, the grip force influences the magnitude of MI for larger frequency ranges and the influence is greater than for the push force.

Since the curves are clustered according to one force while the other force is aggregated across its measured range, the comparison with the ISO 10068:2012 [26] validity range should be interpreted with this aggregation in mind. An assessment of the validity range of ISO 10068:2012 shows that, in Figure 4, the four lowest curves (10, 21, 32, and 43 N) fall within the ISO specification for push force. However, these MI magnitude values lie below the ISO range. For grip force, the ISO validity range applies to the second to fourth lowest force levels in Figure 5, corresponding to 24–66 N. These MI magnitude values are below the ISO range between 30 and 60 Hz. The median MI magnitude values for varying push forces in Figure 4 are outside the ISO range for low push forces between 35 and 70 Hz and around the second maximum at approximately 85 Hz. These frequency ranges coincide with those in which push force has the strongest influence on the magnitude of MI. The 5th to 95th percentile range also exceeds the ISO range in these regions. Based on the values obtained in this study, ISO 10068:2012 agrees best with push forces between 54 and 76 N. Overall, the deviation from ISO 10068:2012 is smaller for varying push forces than for varying grip forces. For low and high grip force levels, the magnitude of MI exceeds the literature-based ISO values, particularly between 20 and 100 Hz and above approximately 250 Hz, as shown in Figure 5. These frequency ranges correspond to those in which grip force has the strongest influence on the magnitude of MI.

3.1.3. Influence of push and grip forces on the VPA

The VPA is shown in Figures 6 and 7. Accordingly, the figures show the VPA in W for varying push forces from 10-110 N in Figure 6 and varying grip forces from 10-135 N in Figure 7.

In Figures 6 and 7, the VPA curves also vary with different push and grip forces. The progression of the VPA curves is similar for both forces. At 10 Hz the values are between 0.1 and 0.12 W and increase until they reach their maximum between 35-40 Hz. Subsequently, the curves decline and approach zero above frequencies of 100 Hz. For

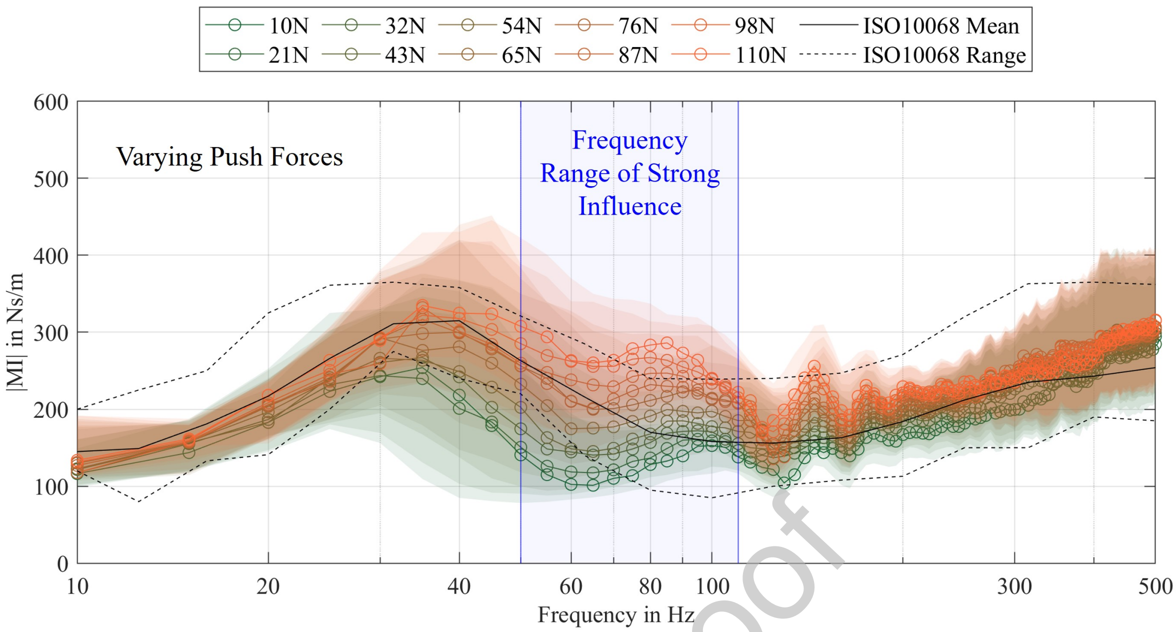

Figure 4: The magnitude of the median mechanical impedance (MI) of the subjects over the frequency range for constant push force levels. For direct comparison the mean values and the range of ISO 10068:2012 are added in black. The frequency range in which the influence of the push force leads to a strong broadening of the median MI magnitude curves is highlighted in blue.

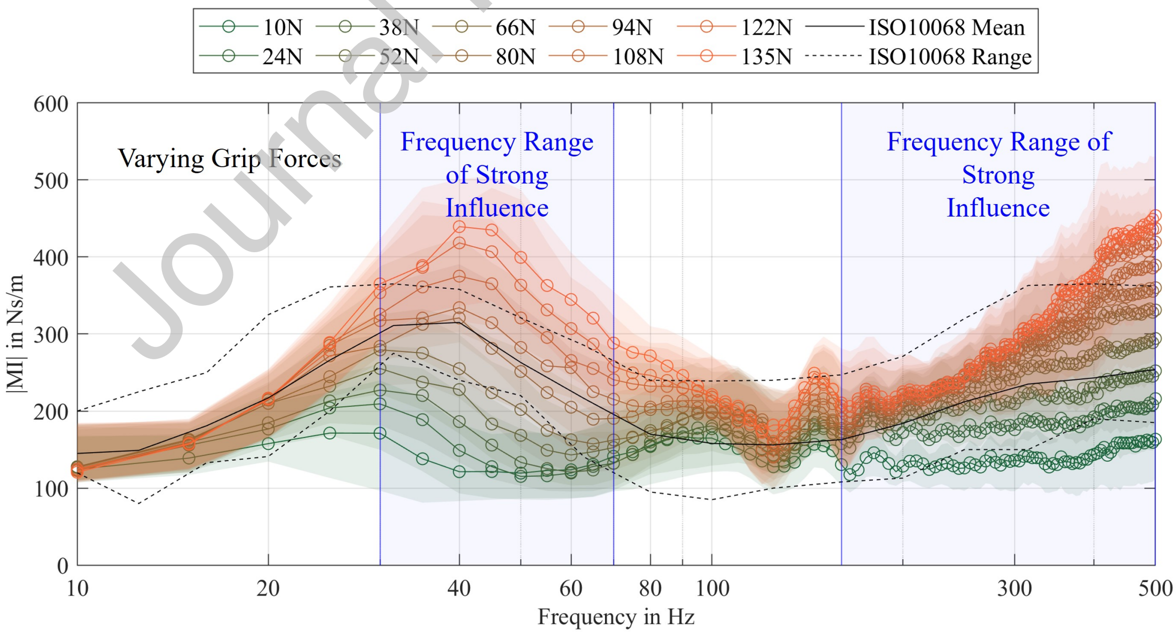

Figure 5: The magnitude of the median mechanical impedance (MI) of the subjects over the frequency range for constant grip force levels. For direct comparison the mean values and the range of ISO 10068:2012 are added in black. The frequency ranges in which the influence of the grip force leads to a strong broadening of the median MI magnitude curves are highlighted in blue.

increasing push forces the VPA increases between 10-15 Hz and 30-500 Hz, while this is the case for grip forces between 30-500 Hz. The opposite occurs with increasing push forces within the frequency range of 20-30 Hz and increasing grip forces between 10-30 Hz. In Figure 7 the maximum shifts to higher frequencies for increasing grip forces. In Figure 6 all VPA curves reach their maximum at 30 Hz without a significant difference in the VPA values. Although the above described trend is partially reversed, the VPA curves follow an almost linear behavior between the force levels for each frequency. Notably, this is not consistent at 35 Hz for both grip and push forces. Within the frequency range of 35 to 60 Hz the VPA curves span the widest range, indicating the greatest variability in values. The largest differences between the VPA curves for varying forces occur at 40 Hz with a value difference of 0.0633 W for push force levels and 0.16 W for grip force levels. Thus, the observed VPA spread is larger for varying grip force than for varying push force in the frequency range with the highest variability. For subject 1 the VPA has its highest broadening with an increase by 8.3 times at 30 Hz.

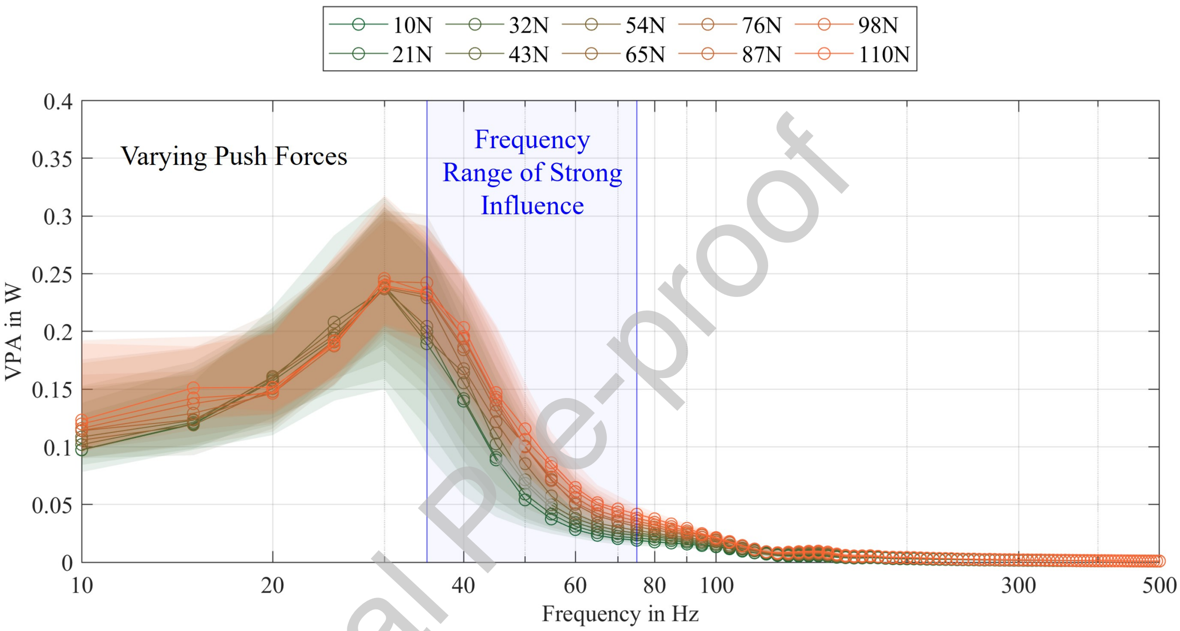

Figure 6: The median vibration power absorption (VPA) of the subjects over the frequency range for constant push force levels. A higher push force usually also leads to higher VPA values, but for frequencies between 20-30 Hz the trend is reversed. The frequency range in which the influence of the push force leads to a strong broadening of the median VPA curves is highlighted in blue.

3.2. RQ2: How many discrete levels of push or grip force are required to predict the mechanical impedance and vibration power absorption at intermediate force levels within the investigated force range with an accuracy of at least 95 %?

The interpolation is conducted for all possible combinations of push and grip forces with two, three and four grids as shown in Table 3. The interpolations of the magnitude of MI and VPA are combined and are listed as mean error metrics for each subject in Tables 5 and 6. The mean values of the interpolations of the magnitude of MI are summarized for each subject in Table 5. The mean values of the deviation from the interpolation and the measurement of the VPA for each subject are given in Table 6. Additionally, the rows named subject *1-5, aggregated* are based on all measurements of the individual subjects. The rows named *Mean* are the summarized mean error value of the 5 subjects individually. The table is categorized by the number of grid curves.

Figure 8 visualizes an example of the interpolation carried out using different numbers of grid curves. The figure shows the magnitude of MI over the frequency range of 10 to 500 Hz. MI magnitude curves in green are recorded with the lowest force value, the higher the force gets the more the color changes to orange. The shaded area corresponds to the 5th to 95th percentile of the same colored force. The number of curves per figure depends on the number of the grid curves. In addition, the interpolated curve is shown in pink, as well as the measured magnitude of MI curve

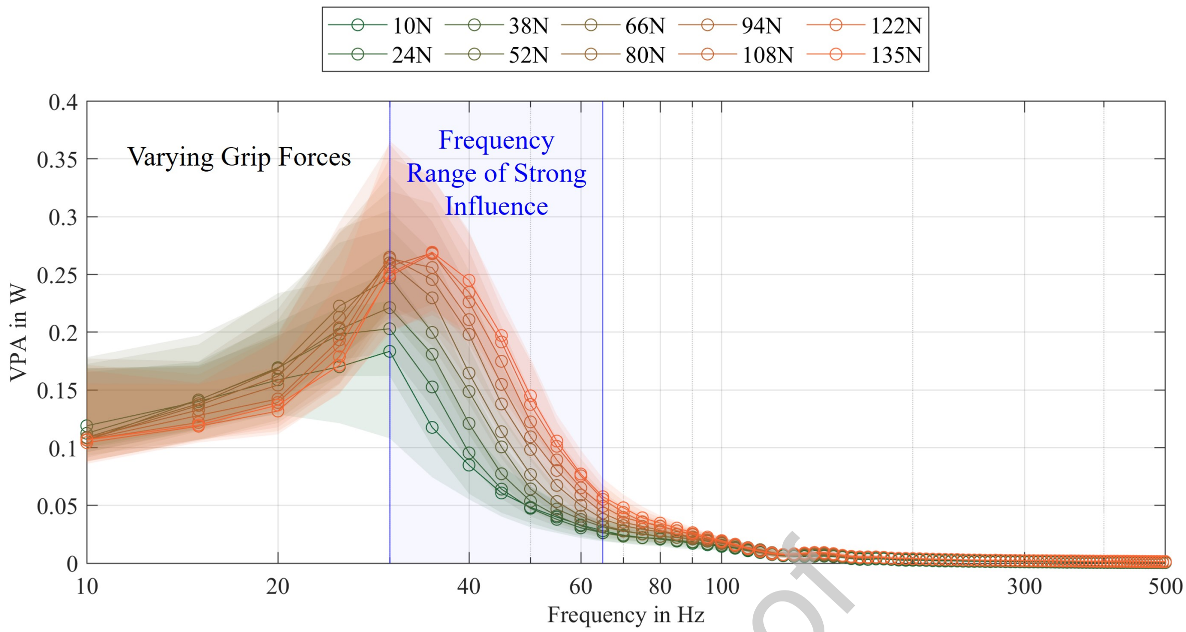

Figure 7: The median vibration power absorption (VPA) of the subjects over the frequency range for constant grip force levels. A higher grip force usually also leads to higher VPA values, but for frequencies between 10-30 Hz the trend is reversed. The frequency range in which the influence of the grip force leads to a strong broadening of the median VPA curves is highlighted in blue.

Table 4
Corresponding error metrics for the prediction of the mechanical impedance of 52 N grip force in Figure 8.

Subject	Predicted force	Grids	RMSE in Ns/m	RRMSE in %	MAPE in %
1-5, aggregated	Fg 52 N	2	26.13	11.47	9.90
		3	12.17	5.34	4.75
		4	6.09	2.67	2.33

of the desired force for comparison in blue with the 5th to 95th percentile as shaded area in blue. In Figure 8 the interpolated magnitude of MI curve is a grip force of 52 N for the curves of subjects 1 to 5. In a) two grid curves are utilized for the percentage-based interpolation, while in b) four grid curves are used. The interpolated curve has a similar progression compared to the measured curve over the entire frequency range. The interpolated curves generally reproduced the frequency-dependent shift of local maxima and minima and remained within the 5th–95th percentile range of the corresponding measured curves. In a) the interpolated and the measured MI magnitude curves vary in the frequency ranges of 45 to 80 Hz and 200 to 500 Hz the most. For a better assessment of the actual deviation, the error metrics for this interpolation are listed in Table 4. It can be seen that each error metric achieves lower values with a higher number of grid curves. The MAPE metric does not weight the error and is visually good comparable to the curves in Figure 8. The interpolation with two grid curves results in a MAPE of 9.90 %, with adding one more grid curve the value decreases to 4.75 % and with four grid curves the value reaches 2.33 %. With four grid curves the interpolated values only deviate from the measured values by an RMSE value of 6.09 Ns/m for each frequency. The percentage error metrics are 2.33 % for the MAPE and 2.67 % for the RRMSE.

The error analysis in Table 5 of predicting the magnitude of MI shows that the mean error values vary between the subjects. The highest and lowest error values of the subjects change with the number of grid curves. For example, subject 5 has low error metrics for two grid curves compared to the remainder, but for three and four grid curves the error values of subject 5 are in the middle range. The subjects individual MI magnitude progression differs as shown in Figure 2, their summary as subject 1-5 with a higher number of measurements enables the best interpolation

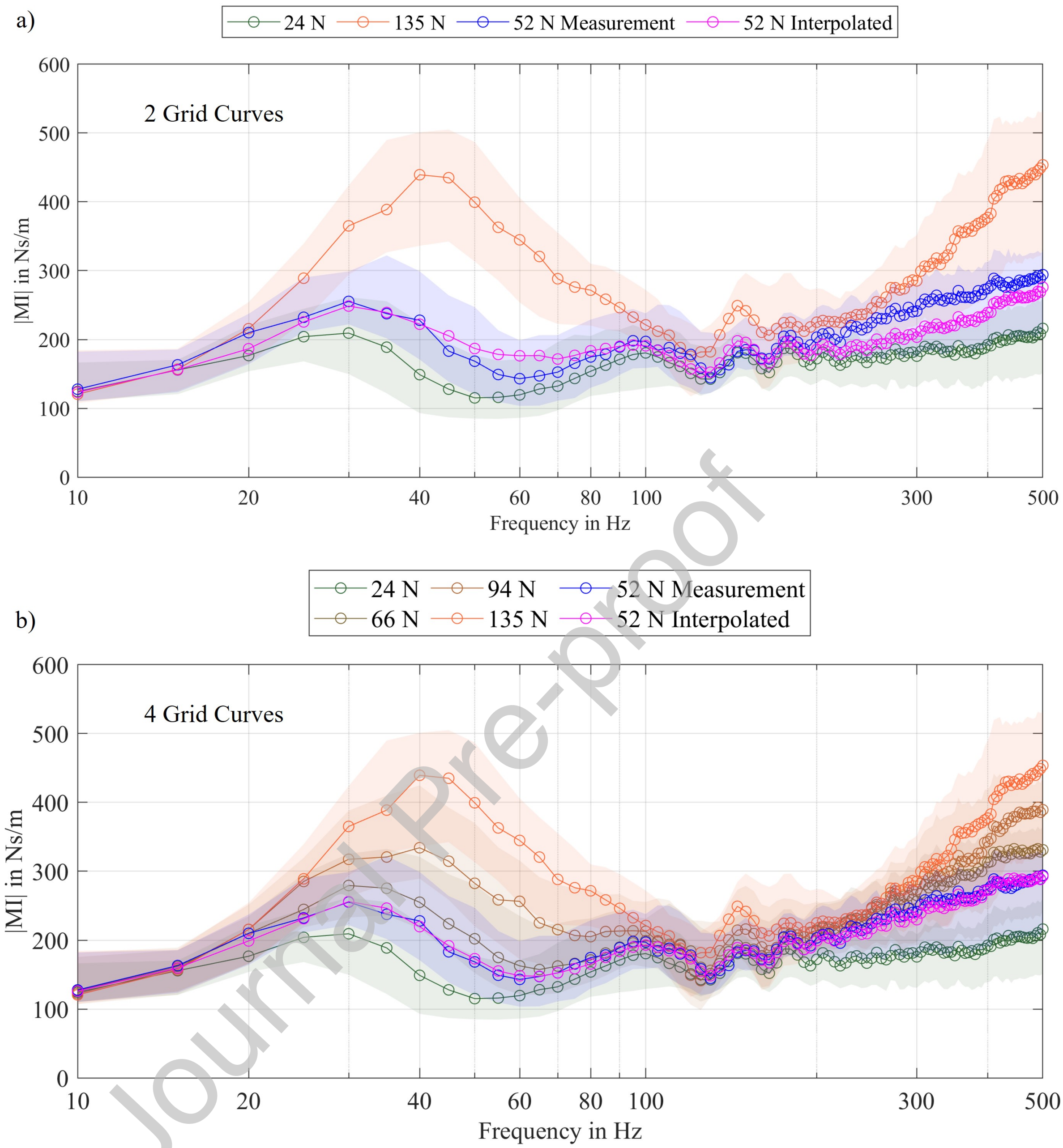

Figure 8: The figures exemplary show the interpolated magnitude of MI curve in pink for a grip force of 52 N over the frequency range. For validation the corresponding measured values are added in blue, the solid curve shows the median and the shaded area the 5th to 95th percentile. In a) two and in b) four grid curves are used to interpolate between the median curves of the subjects. The interpolations are within the 5th to 95th percentile (blue) of corresponding measured values. With four grid curves the deviation from the interpolated (pink) to the measured curve (blue) is less than with two grid curves.

results for three and four grid curves. The difference between RRMSE and MAPE is around 1 %, which is comparably small, although RMSE and RRMSE are sensitive to outliers due to squaring the error values, while the error weighting of MAPE is linear. With three grid curves the average RMSE is 11.42 Ns/m, while the mean MAPE is 3.72 %. In particular, subject 4 shows the lowest error deviation with an RMSE of 9.60 and a MAPE of 2.77 %. With four grid curves, the error analysis shows a significant improvement in prediction accuracy compared to two and three grid curves. The average RMSE is reduced to 10.20 Ns/m, while the mean MAPE is 3.29 %. The higher the amount of

Table 5
Error metrics for the prediction of the mechanical impedance with varying amounts of grid curves. The values listed are the mean values of all possible interpolations for the specific amount of grid curves and subjects. The first five rows with metric values are the mean values of the subject individually. In the row named *1-5, aggregated* the measurement data of all subjects are summarized and used for the interpolation described in this paper. The row *mean* takes the mean value of all the above.

Error metrics for the prediction of the magnitude of MI with varying amounts of grid curves			
2 grid curves			
Subject	RMSE in Ns/m	RRMSE in %	MAPE in %
1	19.74	6.49	5.72
2	17.33	8.32	7.20
3	23.08	7.85	6.03
4	17.36	6.40	5.22
5	15.52	8.37	6.58
1-5, aggregated	16.93	6.85	5.60
Mean	18.33	7.38	6.06
3 grid curves			
Subject	RMSE in Ns/m	RRMSE in %	MAPE in %
1	12.86	4.28	3.82
2	11.31	5.46	4.37
3	13.67	4.70	3.34
4	9.60	3.56	2.77
5	11.96	6.52	4.89
1-5, aggregated	9.12	3.77	3.11
Mean	11.42	4.71	3.72
4 grid curves			
Subject	RMSE in Ns/m	RRMSE in %	MAPE in %
1	12.24	4.06	3.44
2	11.14	5.40	4.23
3	11.28	3.85	2.83
4	9.34	3.50	2.66
5	10.38	5.68	4.30
1-5, aggregated	6.83	2.83	2.28
Mean	10.20	4.22	3.29

grid curves, the better the error values get. The greatest difference emerges from two to three grid curves. Also a bigger data base (subjects 1-5, aggregated) leads to better results. With three and four grid curves the interpolation reaches percentage errors of less than 5 %.

Table 6 lists the error metrics for the interpolation of the VPA. The table shows the mean values of each subject individually as well as the summary of all measurements of subjects 1-5. The rows named *Mean* include the mean values of the errors listed above. Likewise the error metrics for the magnitude of MI interpolation, the greatest decrease in the overall mean values can be seen from two to three grids. From three to four grids the errors become lower but less pronounced. Here as well, the subject with the best interpolation with two grid curves does not necessarily lead to the lowest values with three or four grid curves. In contrast to the prediction of the magnitude of MI the RRMSE and the MAPE value have a different order of magnitude. The outlier sensitive RRMSE is around four times higher than the MAPE for all amounts of grid curves. The interpolation of VPA curves is less accurate than for the MI magnitude values, especially in the outlier sensitive error metrics. Still, the MAPE for three and four grid curves reaches values below 5 %.

Table 6
Error metrics for the prediction of the vibration power absorption with varying amounts of grid curves. The values listed are the mean values of all possible interpolations for the specific amount of grid curves and subject. The first five rows with metric values are the mean values of the subject individually. In the row named *1-5, aggregated* the measurement data of all subjects are summarized and used for the interpolation described in this paper. The row *mean* takes the mean value of all the above.

Error metrics for the prediction of the VPA with varying amounts of grid curves			
2 grid curves			
Subject	RMSE in W	RRMSE in %	MAPE in %
1	0.00661	24.28	6.21
2	0.00492	24.70	7.35
3	0.007505	30.34	6.48
4	0.00415	19.14	5.51
5	0.00392	22.71	6.44
1-5, aggregated	0.00341	16.46	5.60
Mean	0.00509	22.94	6.27
3 grid curves			
Subject	RMSE in W	RRMSE in %	MAPE in %
1	0.00355	13.29	3.41
2	0.00243	12.29	4.97
3	0.00438	17.92	3.46
4	0.00261	12.28	2.94
5	0.00278	16.29	5.03
1-5, aggregated	0.00162	7.92	2.94
Mean	0.00289	13.33	3.79
4 grid curves			
Subject	RMSE in W	RRMSE in %	MAPE in %
1	0.00400	14.89	2.99
2	0.00218	10.98	4.80
3	0.00365	14.91	3.13
4	0.00257	12.31	2.69
5	0.00225	13.13	4.60
1-5, aggregated	0.00140	6.82	2.25
Mean	0.00267	12.17	3.41

4. Discussion

4.1. RQ1: How do different push and grip forces influence the mechanical impedance and vibration power absorption along the translational z_h-axis of the hand-arm system?

4.1.1. Distribution due to grip and push force variation and inter-subject variability

The results of this study support the current state of research that push and grip force influence both MI and VPA. The fluctuations in magnitude of MI and VPA across frequencies also depend on the inter-subject variability, like anthropometry. Within a given subject, the force-dependent spread was substantial, with the magnitude of MI reaching up to 15.8 times higher values and VPA reaching up to 8.3 times higher values at the same frequency.

The variance in the median values for VPA and magnitude of MI between subjects can be caused by many possible influencing factors. The measurements in this study can provide further evidence. Relevant factors include, for example, the anthropometry of the subjects, their physical condition, fatigue and the posture during the data acquisition [21].

The curves of the two female subjects (2 and 5) differ from those of the other subjects. This observation is consistent with Bylund et al. [9], who observed higher VPA values in men than in women; however, this effect was no longer significant after correction for anthropometric data. Vincent et al. [44] also reported sex-related differences in the biodynamic response of the HAS, particularly in the lower natural-frequency modes, which remained significant for the first two modes after adjusting for age, hand length, palm width, and body mass index. Together, these findings suggest that subject-specific characteristics may contribute not only to the magnitude of MI and VPA, but also to shifts in characteristic frequency-dependent features of the MI magnitude curve, such as the global maximum and the local minimum around 60–70 Hz.

The observations in this study show a possible connection between the higher hand mass of subject 1 and subject 4 and the shift of the global maximum toward lower frequencies. One possible explanation is that higher force values modify the vibration behavior of the HAS, so that, as forces increase, the resistance to vibrations increases. This can lead to 15 times higher resistance to vibrations at higher forces than at lower forces.

According to Lindenmann et al. the waviness in the magnitude of MI above 150 Hz can be explained by an upswing at individual frequencies, which causes a local change in the mechanical preload of the vibrating tissue [30]. This can cause the magnitude of MI to vary for individual frequencies. Another theory is that the tonic vibration reflex could also cause the waviness [19, 20].

The higher VPA values for subject 1 are due to the settings used during data collection. Here, the RMS of acceleration in the time domain was set 1.1 times higher than for the remaining subjects. This can be explained by the higher energy input, since the velocity at the excitation point is included quadratically in the calculation of the VPA. Increasing forces can lead to the HAS absorbing eight times more energy.

4.1.2. Influence of push and grip forces on the MI

The already known stronger effect of grip forces compared to push forces can be confirmed [30]. For the magnitude of MI push forces have their strongest effects in the mid-range (50–110 Hz), while grip forces predominantly influence the magnitude of MI between 30–70 Hz and 160–500 Hz. The behavior of the magnitude of MI between the lowest and highest force measurements is approximately linear, see Figures 2, 4 and 5. The observed approximate linearity therefore refers to local interpolation between measured force levels, whereas the combined biomechanical effect of push and grip force remains nonlinear and non-additive.

The effects of push and grip forces overlap for certain frequency ranges. An increase in the push force causes an increase in the magnitude of MI, although the influence is less than for the grip force. With varying forces the stiffness and damping properties of the HAS change. While the grip forces are generated in the hand, they primarily affect the hand and forearm, the push force mainly affects the upper arm and is generated out of the shoulder. At higher frequencies, the vibration transmission to areas further away from the hand decreases, as less tissue is involved in the vibration event. Accordingly, the effect of push force is lower at higher frequencies. Below approximately 200 Hz, however, the results indicate that grip and push forces are of nearly equal importance, reflecting the mechanical coupling of the hand-arm structure with the handle [33]. At frequencies above 200 Hz, the biodynamic response of the HAS is more strongly influenced by grip force, which may be explained by stronger mechanical coupling and a larger effective contact area at the hand–handle interface [33]. The increasing MI magnitude values for higher grip forces can be explained by an increasing stiffening of the HAS resulting from the increased muscle contraction. At the same time, higher grip forces may increase vibration transmission from the hand to the forearm by increasing the mechanical coupling between the hand, handle, and adjacent soft tissues. This leads to a higher vibration transmission to the upper arm and shoulder. **This altered coupling condition may also explain why the effect of push force is more pronounced at high grip forces, whereas it is less pronounced at low grip forces.**

The influence of the push and grip forces is differently pronounced. The variation of the grip forces leads to a greater dispersion of the MI magnitude curves. In the investigated range, varying grip force increased MI magnitude values by up to approximately a factor of three, whereas varying push force increased MI magnitude values by up to approximately a factor of two. The visible gap between 66 N and 80 N grip force in Figure 5 could be due to the summary of all 1500 measurements of the individual subjects

[12]. With a higher number of measurements and subjects this effect presumably is reduced. It can also be seen that the effect of push and grip forces leads to an approximately linear behavior of the MI magnitude curves. **It is therefore possible that the behavior is linear with a larger sample. It is also remarkable that the global maximum shifts to a higher frequency with increasing forces.** If the behavior of a single-mass oscillator is considered as a simplified approach, with a higher stiffness value of the HAS the resonance frequency increases, which is presumably the reason for the maximum shift.

The median curves in Figure 5 were calculated from measurements with constant push force but varying grip forces between 10 and 135 N. Thus, the average grip force is approximately 73 N, which exceeds the ISO validity range and would be expected to increase the magnitude of MI. Conversely, the average push force in Figure 4 is approximately

60 N and therefore close to the ISO validity range. Nevertheless, the measured MI magnitude curves within the ISO validity range remain below the ISO curve. Acceleration cannot explain these lower MI magnitude values, since the RMS acceleration of the multisine signal was 30 m/s^2, which is higher than in most studies used to derive the ISO range. The broad spread of the measured curves is instead mainly attributable to the wider force range investigated in this study, especially for grip force. The observed deviations agree with Lindenmann et al., who reported both underestimation and overestimation of ISO reference values [30]. The frequency ranges with strong force influence also largely match their reported effect sizes for push and grip force [10, 30]. The increased MI with increasing grip force is further consistent with Pan et al. [39] and Lundstroem et al. [32]. The comparison with ISO 10068:2012 shows that standardized MI representations have limited applicability when grip and push forces deviate from the force ranges covered by the standard [26]. **The MI strongly depends on the forces exerted by the subject, among other factors. If the forces used for the reference measurement are different, the MI can deviate significantly from the reference. This emphasizes that forces should not be treated as a boundary condition but as a modeling parameter when MI is used for analysis, comparison, or risk assessment.**

4.1.3. Influence of push and grip forces on the VPA

Push and grip forces have a strong frequency-dependent influence on the VPA. In the frequency range with the largest VPA variability, the effect of grip force was greater than that of push force, indicating that grip force is the dominant coupling-force parameter for absorbed vibration power. Over wide frequency ranges, higher forces lead to increased energy absorption in the hand-arm system, whereas in the frequency range of approximately 10–30 Hz, a reverse effect occurs and higher forces reduce absorption. Overall, the force-dependent VPA response is approximately linear at most frequencies, with a few frequency-specific nonlinear deviations.

The course of the obtained VPA values corresponds approximately to that known in the literature [2, 4, 3, 15]. The behavior of the VPA between the lowest and highest force measurements is approximately linear per frequency between 35 and 500 Hz, see Figures 3, 6 and 7. However, the VPA magnitude is approximately one order of magnitude higher than values reported in some previous studies, likely due to the high vibration dose used here [2, 4]. In the literature the common root-mean-square acceleration for single sine is often between 2.5-9 m/s², while here it is 30 m/s². It is also known that the VPA increases with a higher vibration dose [7, 4]. In contrast, Dong et al. reported VPA values that are up to ten times higher than those presented here. This discrepancy arises from differences in the calculation method: Dong et al. determined the VPA for individual substructures and subsequently summed them with an acceleration of 10 m/s² [15].

Similar force-dependent trends have been reported in previous studies. Aldien et al. have demonstrated a significance for the frequencies above 40 Hz [4]. Similar to here, they also found that the force influence is low for frequencies higher than 200 Hz. For most frequencies a higher push or grip force leads to an increased energy absorption to the HAS. This trend is reversed for push forces between a frequency of 20-30 Hz, which results in less absorption, see Figure 6 and for grip forces between 10-25 Hz, compare Figure 7. Burstroem and Lundstroem also reported the reversed trend for frequencies below 16 Hz, which is only valid for the effect of grip forces in this contribution [8]. In another publication of Burstroem et al. the same method was used, but they have not found the same effect, most likely due to the different posture [6]. Aldien et al. analyzed three levels of push and grip force and also found that with an increased force in these frequency ranges the VPA decreases while it increases for the remaining frequencies [4, 3]. In their analyzes the frequency after which an increasing force resulted in an increased VPA was at 40 Hz, while in this contribution the reversal point is at 30-35 Hz. They could not show a significant trend for frequencies below 40 Hz, this may be due to the comparatively low acceleration of 2.5 m/s².

A possible biomechanical explanation is that higher forces cause the HAS to stiffen, which means that more energy is reflected and less energy can be absorbed. The extent to which the vibration excitation is transmitted through the HAS depends on the frequency. Frequencies smaller than 25 Hz are transmitted to the arms and shoulder, while frequencies above 100Hz only have an impact to the hand which comprises the measuring handle [40, 1, 2]. This means that for relevant frequencies of the upper arm and forearm a higher force leads to less absorption. For the frequencies relevant for the anterior part of the forearm and the hand a higher push and grip force increases the energy absorption into these substructures.

The frequency ranges with the highest influence of push and grip forces on the VPA differ from the ones of the MI. The VPA is most influenced by varying push forces between 10-20 Hz and 30-80 Hz, while the grip force influences the frequencies from 10-70 Hz the most. Beside of the frequency range of 35-40 Hz for push forces and at 10 Hz and between 25-30 Hz for grip forces, the influence of the push and grip forces on the VPA can be approximated as linear per frequency. This can be supported by the studies of Aldien et al., which showed a nearly linear increase of the VPA with the push forces between 31.5-1000 Hz [4]. However, this approximate linearity describes the local force-dependent trend at individual frequencies, while the combined influence of push and grip force remains interaction-dependent. Most of the vibration power is absorbed for frequencies up to 60 Hz, this is the frequency range where hand-held tools transmit vibrations to the HAS predominantly [21, 41], which possibly leads to an increased health risk.

4.2. RQ2: How many discrete levels of push or grip force are required to predict the mechanical impedance and vibration power absorption at intermediate force levels within the investigated force range with an accuracy of at least 95 %?

In this study, three grid curves were sufficient to predict intermediate force levels with a mean MAPE below 5 % for both the magnitude of MI and VPA, corresponding to high accuracy for MI and acceptable prediction accuracy for VPA. A fourth grid curve further reduced the error but provided only a smaller additional improvement.

This has important implications for experimental efficiency, as the force-dependent behavior of the hand-arm system can be determined within a limited operating range with relatively few reference conditions, provided that the force levels are distributed across the range examined. The current results suggest that the underlying force-reaction relationship exhibits sufficient regularity to support interpolation-based approaches, at least for certain force conditions. For the magnitude of MI the MAPE and RRMSE differ by 1 %, indicating that only weak outliers can be expected in the prediction of the magnitude of MI. For VPA, the RRMSE values are almost four times the size of the MAPE values, which indicates possible outliers by linear interpolation for intermediate VPA values. Compared to the magnitude of MI, the lower predictability of VPA is related to its mathematical description. VPA depends not only on impedance, but also on velocity and phase relationships at the excitation point, making it more sensitive to measurement variations, localized response characteristics, and outliers. As a result, interpolation errors are expected to be increased. This sensitivity underscores the importance of cautious interpretation when interpolated VPA values are used for exposure assessment or health-related modeling. The observed standard deviations of the repeated MI and VPA measurements further show that measurement disturbances should be minimized and that repeated measurements remain important when deriving interpolation-based predictions. The influence of individual subjects should not be underestimated. Although the results of this study suggest that aggregating subjects can partly compensate for individual differences, this may still lead to inaccurate predictions for individuals whose anthropometric characteristics deviate from the group. This indicates that subject-specific parameters should be considered in future models, especially when individual exposure or individual biodynamic response is of interest.

The results of the interpolation allow a statement to be made about the compromise between prediction accuracy and the number of measurements required. Adding additional force levels reduces the interpolation distances and partially compensates for non-linearities and interactions between push and grip forces. However, beyond a certain point, further refinement results in only minor improvement in the measured error. This suggests that for many applications, a limited number (three grid curves) of carefully selected force conditions may be sufficient to capture force-dependent effects, while excessive sampling in relation to the required measurement effort offers only minor additional benefits.

From a modeling perspective, this behavior can be interpreted as a consequence of changes in effective stiffness, damping, and contact conditions as force increases. Although the hand-arm system is biomechanically complex and inherently nonlinear, averaging across repetitions and subjects appears to attenuate local nonlinearities, resulting in response characteristics that can be well predicted by low-order models. This observation is consistent with previous work showing that biodynamic responses, despite their physiological complexity, often exhibit quasi-linear trends when studied under controlled conditions [30]. Overall, these considerations suggest that interpolation-based prediction of force-dependent biodynamic measures is a useful and efficient strategy, provided its limitations are recognized. Overall, these considerations suggest that interpolation-based prediction of force-dependent biodynamic measures is a useful and efficient strategy, provided its limitations are recognized. The main methodological advance of this study is the demonstration, using a systematic 10×10 grip–push force grid, that MI and VPA can be predicted at intermediate force levels from as few as three discrete reference force levels with an accuracy of about 95 %. This goes beyond previous studies with only few discrete force combinations and enables a substantial reduction in experimental effort while preserving the main force-dependent characteristics of the HAS. Future studies could further improve robustness and generalizability by combining interpolation approaches with subject-specific parameters.

4.3. Limitations

As described in Section 2.3, the 1500 measurements were grouped for comparability. Grouping the measurements into medians per force level shows that the median of the other force lies behind the curves displayed. For example, the magnitude of MI increases more sharply for increasing push forces with higher than with lower grip forces. This suggests that the forces cannot be considered independently of each other. To present the results more clearly, the 100 factor combinations were structured through clustering. The curves are therefore valid around the median force level of the force value. Consequently, the displayed force-specific curves describe aggregated trends rather than the full interaction surface of all 100 push–grip force combinations. For higher and lower values of the other force the effects slightly differ. The whole data set is published in [12]. Behind every curve in the shown figures, there are 150 to 300 measurements, this could neglect other trends, even though the 5th to 95th percentile is shown additionally to minimize the effect. The study was conducted with only 5 subjects, more subjects could lead to more or less significant as well as different effects. Likely, more subjects would lead to a linear behavior between the upper and lower force levels per frequency. No professional hand-held tool users participated in this study. To accomplish this, sportive subjects were selected, wherefore the order of magnitude could differ. Although many breaks were given, fatigue could still have occurred. To eliminate this as far as possible, an exclusion criterion was introduced. Nevertheless, the remaining measurements deviate slightly from the specified force combination. The high level of force required may have led to overloading of the subjects. Even the minimum requirement that the grip and push force of the subjects must be twice as high as the maximum force to be applied may not protect against overloading. The multisine excitation may have influenced the MI and VPA values. The progressions, especially at higher frequencies, are supposed to be smoother. Considering that the values are close to the literature ones, it is assumed that the relationships of MI and VPA to the analyzed factors are justified.

The generalizability of these findings should be demonstrated in a study with a larger sample size; in such a study, only three or four interpolation support points, along with validation measurements, would be required. The interpolation approach should be regarded as valid only within the investigated force range; extrapolation to higher or lower grip and push forces requires additional validation measurements.

5. Conclusion

Taking into account the different combinations of grip and push force, values for the magnitude of MI can be up to 15 times as high at the same frequency within a given subject, while the VPA values can be up to 8 times as high. This force-related change strongly depends on the frequency. In general, variations in grip forces led to higher deviations in the MI magnitude and VPA curves than variations in push forces. Specifically, push force had the strongest influence on the magnitude of MI between 50 and 110 Hz, whereas grip force mainly affected the magnitude of MI between 30 and 70 Hz and between 160 and 500 Hz; for VPA, higher forces generally increased absorption but reduced it in the low-frequency range of approximately 10–30 Hz. Additionally, the investigation shows that the interactions between push and grip forces are non-linear and can therefore not be considered independently.

Based on the systematic investigation of the effects of grip force and push force on MI and VPA using the 10×10 force combination matrix, the influence of grip and push forces on MI and VPA can be approximated as linear per frequency. This was demonstrated in five subjects, for whom linear interpolation provided accurate predictions both when fitted on an individual basis using each subject's own data and when applied to the aggregated data across all subjects for each force combination. In the present study, three grid curves were sufficient to predict MI and VPA at intermediate force levels within the analyzed force range with a mean absolute percentage error below 5 %. An increase to four grid curves further improved prediction accuracy, although the cost–benefit ratio of this additional effort must be weighed up in future studies. This approach shows that, within the investigated force range and sample, MI and VPA curves can be predicted for intermediate grip and push force levels, while the combined influence of both forces should still be considered interaction-dependent. This may support future modeling efforts under varying force conditions.

The comparison with ISO 10068:2012 showed that the measured MI magnitude curves did not consistently fall within the ISO reference range. The largest deviations occurred in frequency ranges where grip and push force had a pronounced influence on magnitude of MI, particularly between 20 and 100 Hz and above approximately 250 Hz. Since VPA depends on MI, these deviations are also relevant for the resulting VPA. This indicates that ISO-based MI and VPA representations should only be applied with consideration of the underlying grip and push force conditions.

Future investigations should validate the presented findings using a larger and more diverse sample and extend the analysis to additional translatory and rotatory directions of the hand–arm system. A reduced number of force levels, identified in this study, may enable such validation studies with substantially lower experimental effort. Further work is required to assess the generalizability of the interpolation approach across different user populations and application contexts. Furthermore, frequency-dependent MI and VPA provide a practical basis for early-stage tool and system optimization by anticipating vibration transmission and reducing exposure without compromising usability. A key outlook is the development of physical and simulation-based hand–arm models that incorporate operating parameters such as grip and push forces—enabling automated testing (e.g., robotic replication of human dynamics) and virtual frontloading under controlled conditions, including systematic edge-case evaluation.

Declaration of Interest

The authors declare that they have no known competing financial interests or personal relationships that could have appeared to influence the work reported in this paper. Therefore, we declare no conflicts of interest.

6. Acknowledgment

This research is funded within the proposals "Modeling and simulation of the vibration behavior of hand-arm systems for six excitation directions in the context of user-centered product development" (527244581) and "Dynamically adaptive impedance elements for influencing vibrations in validation environments" (530564503) by the German Research Foundation (DFG). The test equipment was partially supported through the funding of the DFG under proposal 275571425. The research results are the sole responsibility of the authors and do not represent the official opinion of the DFG.

7. Declaration of generative AI and AI-assisted technologies in the writing process

During the preparation of this work, the authors used Deepl SE and ChatGPT4 to improve writing and language skills. After using these tools, the authors reviewed and edited the content as needed and assume full responsibility for the content of the publication.

CRediT authorship contribution statement

Carina Spengler: * Conceptualization, Data curation, Investigation, Software, Visualization, Formal analysis, Methodology, Validation, Writing – Original Draft. **Simon Saurbier:** * Conceptualization, Data curation, Investigation, Software, Visualization, Formal analysis, Methodology, Validation, Writing – Original Draft. **Andreas Lindenmann:** Software, Writing – Review & Editing . **Markus Doellken:** Writing – Review & Editing. **Lukas Bunk:** Writing – Review & Editing. **Dieter Krause:** Writing – Review & Editing. **Sven Matthiesen:** Supervision, Funding.* These authors contributed equally to this work and share first authorship.

References

[1] Adewusi, S., Rakheja, S., Marcotte, P., Boutin, J., 2010. Vibration transmissibility characteristics of the human hand–arm system under different postures, hand forces and excitation levels. Journal of Sound and Vibration 329, 2953–2971. doi:10.1016/j.jsv.2010.02.001.

[2] Adewusi, S., Rakheja, S., Marcotte, P., Thomas, M., 2013. Distributed vibration power absorption of the human hand-arm system in different postures coupled with vibrating handle and power tools. International Journal of Industrial Ergonomics 43, 363–374. doi:10.1016/j.ergon.2013.04.004.

[3] Aldien, Y., Marcotte, P., Rakheja, S., Boileau, P.É., 2006a. Influence of hand–arm posture on biodynamic response of the human hand–arm exposed to zh-axis vibration. International Journal of Industrial Ergonomics 36, 45–59. doi:10.1016/j.ergon.2005.07.001.

[4] Aldien, Y., Marcotte, P., Rakheja, S., Boileau, P.É., 2006b. Influence of hand forces and handle size on power absorption of the human hand–arm exposed to zh-axis vibration. Journal of Sound and Vibration 290, 1015–1039. doi:10.1016/j.jsv.2005.05.005.

[5] Besa, A.J., Valero, F.J., Suñer, J.L., Carballeira, J., 2007. Characterisation of the mechanical impedance of the human hand–arm system: The influence of vibration direction, hand–arm posture and muscle tension. International Journal of Industrial Ergonomics 37, 225–231. doi:10.1016/j.ergon.2006.10.019.

[6] Burström, L., 1994. The influence of biodynamic factors on the absorption of vibration energy in the human hand and arm. Nagoya journal of medical science 57, 159–167. URL: https://pubmed.ncbi.nlm.nih.gov/7898572/.

[7] Burström, L., Bylund, S.H., 2000. Relationship between vibration dose and the absorption of mechanical power in the hand. Scandinavian Journal of Work, Environment and Health doi:10.5271/sjweh.507.

[8] Burström, L., Lundström, R., 1988. Mechanical energy absorption in human hand-arm exposed to sinusoidal vibration. International archives of occupational and environmental health 61, 213–216. doi:10.1007/BF00381021.

[9] Bylund, S.H., Burström, L., 2003. Power absorption in women and men exposed to hand-arm vibration. International archives of occupational and environmental health 76, 313–317. doi:10.1007/s00420-002-0410-9.

[10] Cohen, J., 1992. Statistical Power Analysis. Current Directions in Psychological Science 1, 98–101. doi:10.1111/1467-8721.ep10768783.

[11] Cristea, A.F., Blcu, M.C., Haragâș, S., 2025. A Chronological Review of the Transmission and Effects of Mechanical Vibrations on the Hand—Arm System in an Occupational Workplace. Applied Sciences 15, 1182. doi:10.3390/app15031182.

[12] [dataset] Spengler, C., Saurbier, S., Matthiesen, S., 2025. Measurements of the Mechanical Impedance and Vibration Power Absorption for Varying Grip and Push Forces. doi:10.35097/uwz0qdyzh8h8uekw.

[13] Deutsches Institut für Normung e.V., 2013. DIN 45679:2013-02 Mechanische Schwingungen - Messung und Bewertung der Ankopplungskräfte zur Beurteilung der Schwingungsbelastung des Hand-Arm-Systems [DIN 45679:2013-02 Mechanical vibration - Measurement and evaluation of coupling forces for assessment of vibration exposure of the hand-arm system]. doi:10.31030/1930267.

[14] Deutsches Institut für Normung e.V., 2022. DIN EN ISO 10819:2022-12 Mechanische Schwingungen und Stöße - Hand-Arm-Schwingungen - Messung und Bewertung der Schwingungsübertragung von Handschuhen in der Handfläche (ISO 10819:2013 + Amd.1:2019 + Amd.2:2021); Deutsche Fassung EN ISO 10819:2013 + A1:2019 + A2:2022 [Mechanical vibration and shock - hand-arm vibration - measurement and evaluation of the vibration transmissibility of gloves at the palm of the hand (ISO 10819:2013 + Amd.1:2019 + Amd.2:2021); german version EN ISO 10819:2013 + A1:2019 + A2:2022].

[15] Dong, J.H., Dong, R.G., Rakheja, S., Welcome, D.E., McDowell, T.W., Wu, J.Z., 2008. A method for analyzing absorbed power distribution in the hand and arm substructures when operating vibrating tools. Journal of Sound and Vibration 311, 1286–1304. doi:10.1016/j.jsv.2007.10.031.

[16] Dong, R.G., Schopper, A.W., McDowell, T.W., Welcome, D.E., Wu, J.Z., Smutz, W.P., Warren, C., Rakheja, S., 2004. Vibration energy absorption (VEA) in human fingers-hand-arm system. Medical engineering & physics 26, 483–492. doi:10.1016/j.medengphy.2004.02.003.

[17] Dong, R.G., Welcome, D.E., McDowell, T.W., Wu, J.Z., 2013. Modeling of the biodynamic responses distributed at the fingers and palm of the hand in three orthogonal directions. Journal of Sound and Vibration 332, 1125–1140. doi:10.1016/j.jsv.2012.10.003.

[18] Dong, R.G., Wu, J.Z., McDowell, T.W., Welcome, D.E., Schopper, A.W., 2005. Distribution of mechanical impedance at the fingers and the palm of the human hand. Journal of biomechanics 38, 1165–1175. doi:10.1016/j.jbiomech.2004.05.021.

[19] Fattorini, L., Tirabasso, A., Lunghi, A., Di Giovanni, R., Sacco, F., Marchetti, E., 2016. Muscular forearm activation in hand-grip tasks with superimposition of mechanical vibrations. Journal of Electromyography and Kinesiology 26, 143–148. doi:10.1016/j.jelekin.2015.10.015.

[20] Fattorini, L., Tirabasso, A., Lunghi, A., Di Giovanni, R., Sacco, F., Marchetti, E., 2017. Muscular synchronization and hand-arm fatigue. International Journal of Industrial Ergonomics 62, 13–16. doi:10.1016/j.ergon.2016.07.009.

[21] Griffin, M.J., 1990. Handbook of human vibration. 1 ed., Academic Press Limited, London. doi:10.1016/C2009-0-02730-5.

[22] Gurram, R., Rakheja, S., Gouw, G.J., 1995. Mechanical impedance of the human hand-arm system subject to sinusoidal and stochastic excitations. International Journal of Industrial Ergonomics 16, 135–145. doi:10.1016/0169-8141(94)00092-H.

[23] Hamouda, K., Rakheja, S., Marcotte, P., Dewangan, K.N., 2017. Fingers vibration transmission performance of vibration reducing gloves. International Journal of Industrial Ergonomics 62, 55–69. doi:10.1016/j.ergon.2016.11.012.

[24] Heyden, E., Lindenmann, A., Matthiesen, S., Krause, D., 2021. Approach for Calibrated Measurement of the Frequency Response for Characterization of Compliant Interface Elements on Vibration Test Benches. Applied Sciences 11, 9604. doi:10.3390/app11209604.

[25] International Organization for Standardization, 2001. Mechanical vibration - Measurement and evaluation of human exposure to hand-transmitted vibration - Part 1: General requirements (ISO Standard No. 5349-1:2001); German version EN ISO 5349-1:2001. URL: https://www.iso.org/standard/32355.html.

[26] International Organization for Standardization, 2012. Mechanical vibration and shock - Mechanical impedance of the human hand-arm system at the driving point (ISO Standard No. 10068:2012). URL: https://www.iso.org/standard/53714.html.

[27] International Organization for Standardization, 2017. Basic human body measurements for technological design - Part 1: Body measurement definitions and landmarks (ISO 7250-1:2017). URL: https://www.iso.org/standard/65246.html.

[28] Jahn, R., 1985. Einflussgroessen auf die Beschleunigungen elektropneumatischer Bohrhaemmer [Influencing variables on the accelerations of electropneumatic hammer drills]. Dissertation. Universität Dortmund. Dortmund.

[29] Kalra, M., Rakheja, S., Marcotte, P., Dewangan, K.N., Adewusi, S., 2015. Measurement of coupling forces at the power tool handle-hand interface. International Journal of Industrial Ergonomics 50, 105–120. doi:10.1016/j.ergon.2015.09.013.

[30] Lindenmann, A., Schröder, T., Germann, R., Gwosch, T., Matthiesen, S., 2022a. Effect of high level grip-and push force and elevated arm posture on the zh-axis hand-arm impedances. International Journal of Industrial Ergonomics 92, 103375. doi:10.1016/j.ergon.2022.103375.

[31] Lindenmann, A., Uhl, M., Gwosch, T., Matthiesen, S., 2021. The influence of human interaction on the vibration of hand-held human-machine systems - The effect of body posture, feed force, and gripping forces on the vibration of hammer drills. Applied Ergonomics 95, 103430. doi:10.1016/j.apergo.2021.103430.

[32] Lundström, R., Burström, L., 1989. Mechanical impedance of the human hand-arm system. International Journal of Industrial Ergonomics 3, 235–242. doi:10.1016/0169-8141(89)90023-1.

[33] Marcotte, P., Aldien, Y., Boileau, P.É., Rakheja, S., Boutin, J., 2005. Effect of handle size and hand–handle contact force on the biodynamic response of the hand–arm system under zh-axis vibration. Journal of Sound and Vibration 283, 1071–1091. doi:10.1016/j.jsv.2004.06.007.

[34] Matthiesen, S., Lindenmann, A., Bruchmüller, T., 2018a. Anforderungen an ein Messsystem zur Ermittlung der Rotationsimpedanz von Hand-Arm Systemen [Requirements for a measuring system to determine the rotational impedance of hand-arm systems], in: VDI Wissensforum GmbH (Ed.), Humanschwingungen 2018. VDI Verlag GmbH, Düsseldorf. VDI-Berichte, pp. 91–106.

[35] Matthiesen, S., Mangold, S., Bruchmüller, T., 2018b. The influence of variating passive user interactions on power tools in the context of product development. Forschung im Ingenieurwesen 82, 157–168. doi:10.1007/s10010-018-0269-x.

[36] Mishoe, J.W., Suggs, C.W., 1977. Hand-arm vibration part II: Vibrational responses of the human hand. Journal of Sound and Vibration 53, 545–558. doi:10.1016/0022-460X(77)90524-7.

[37] Nilsson, T., Wahlström, J., Burström, L., 2017. Hand-arm vibration and the risk of vascular and neurological diseases - A systematic review and meta-analysis. PloS one 12, e0180795. doi:10.1371/journal.pone.0180795.

[38] Osiak, K., Elnazir, P., Walocha, J.A., Pasternak, A., 2022. Carpal tunnel syndrome: state-of-the-art review. Folia morphologica 81, 851–862. doi:10.5603/FM.a2021.0121.

[39] Pan, D., Xu, X.S., Welcome, D.E., McDowell, T.W., Warren, C., Wu, J., Dong, R.G., 2018. The relationships between hand coupling force and vibration biodynamic responses of the hand-arm system. Ergonomics 61, 818–830. doi:10.1080/00140139.2017.1398843.

[40] Pyykkö, I., Färkkilä, M., Toivanen, J., Korhonen, O., Hyvärinen, J., 1976. Transmission of vibration in the hand-arm system with special reference to changes in compression force and acceleration. Scandinavian Journal of Work, Environment & Health 2, 87–95. doi:10.5271/sjweh.2820.

[41] Radwin, R.G., Armstrong, T.J., Vanbergeijk, E., 1990. Vibration exposure for selected power hand tools used in automobile assembly. American Industrial Hygiene Association journal 51, 510–518. doi:10.1080/15298669091370013.

[42] Rakheja, S., Wu, J.Z., Dong, R.G., Schopper, A.W., Boileau, P.É., 2002. A comparison of biodynamic models of the human hand-arm system for applications to hand-held power tools. Journal of Sound and Vibration 249, 55–82. doi:10.1006/jsvi.2001.3831.

[43] Uhl, M., Bruchmüller, T., Matthiesen, S., 2019. Experimental analysis of user forces by test bench and manual hammer drill experiments with regard to vibrations and productivity. International Journal of Industrial Ergonomics 72, 398–407. doi:10.1016/j.ergon.2019.06.016.

[44] Vincent, M., Engelbrecht, A., Gaudreau, M.A., Legrand, M., Dupont, T., Marcotte, P., 2026. Biodynamic responses of the human hand-arm system under nail gun shock vibration and differences between males and females. International Journal of Industrial Ergonomics 113, 103913. URL: https://www.sciencedirect.com/science/article/pii/S0169814126000363, doi:10.1016/j.ergon.2026.103913.

[45] Wu, J.Z., Welcome, D.E., McDowell, T.W., Xu, X.S., Dong, R.G., 2017. Modeling of the interaction between grip force and vibration transmissibility of a finger. Medical engineering & physics 45, 61–70. doi:10.1016/j.medengphy.2017.04.008.

A. Error metrics for predicting the mechanical impedance for intermediate push and grip force values.

Table A.1
Error metrics for predicting intermediate push forces with 2 grid curves.

Subject	Push Force in N	RMSE in Ns/M	RRMSE in %	MAPE in %
1	32	25.43	8.49	6.90
1	43	10.61	3.62	3.53
1	54	13.55	4.68	4.14
1	65	16.76	5.37	4.33
1	76	16.52	5.21	4.53
1	87	12.63	4.11	3.77
1	98	13.60	4.20	3.40
2	32	20.40	10.27	7.91
2	43	7.51	4.01	3.06
2	54	12.77	6.38	5.36
2	65	9.37	4.75	4.22
2	76	15.63	7.44	6.76
2	87	14.30	6.73	5.11
2	98	11.40	5.30	4.27
3	32	11.69	4.36	3.65
3	43	15.41	5.55	4.29
3	54	22.58	7.91	6.18
3	65	22.34	7.47	4.85
3	76	24.55	7.88	5.62
3	87	20.85	6.65	4.22
3	98	23.04	7.28	3.97
4	32	9.98	3.97	3.01
4	43	9.27	3.62	2.79
4	54	23.64	8.52	5.19
4	65	13.95	5.09	2.87
4	76	11.84	4.23	3.10
4	87	15.45	5.25	3.67
4	98	14.28	4.90	3.60
5	32	12.03	7.05	5.37
5	43	13.63	7.67	4.48
5	54	14.42	7.64	4.64
5	65	18.20	9.51	5.14
5	76	7.16	3.77	2.95
5	87	12.59	6.67	5.39
5	98	12.67	6.35	4.64
1-5, aggregated	32	13.31	5.96	4.53
1-5, aggregated	43	8.48	3.79	3.02
1-5, aggregated	54	10.22	4.43	3.19
1-5, aggregated	65	10.88	4.58	3.63
1-5, aggregated	76	13.46	5.55	4.16
1-5, aggregated	87	12.32	5.00	3.82
1-5, aggregated	98	8.37	3.32	2.74

Table A.2
Error metrics for predicting intermediate grip forces with 2 grid curves.

Subject	Grip Force in N	RMSE in Ns/M	RRMSE in %	MAPE in %
1	38	17.10	7.17	6.42
1	52	22.36	8.60	8.28
1	66	35.39	12.01	10.69
1	80	29.80	9.54	8.61
1	94	32.17	9.39	8.29
1	108	21.54	6.05	5.07
1	122	8.89	2.44	2.13
2	38	15.79	9.50	8.67
2	52	15.56	8.68	7.60
2	66	23.56	11.91	10.70
2	80	30.46	13.90	12.65
2	94	22.80	10.13	9.16
2	108	19.84	8.32	7.55
2	122	23.25	9.19	7.78
3	38	23.31	9.73	8.78
3	52	27.84	10.70	9.47
3	66	29.73	10.59	9.20
3	80	32.81	10.78	8.54
3	94	34.01	10.54	7.76
3	108	21.64	6.57	4.87
3	122	13.27	3.91	3.06
4	38	12.13	5.55	4.96
4	52	23.51	9.80	9.13
4	66	30.75	11.61	10.45
4	80	30.46	10.95	9.99
4	94	22.62	7.82	7.12
4	108	16.60	5.49	4.69
4	122	8.59	2.75	2.45
5	38	9.22	6.55	5.08
5	52	24.31	14.13	12.87
5	66	23.14	12.92	12.09
5	80	21.64	11.44	9.64
5	94	24.74	12.23	10.11
5	108	12.96	6.36	5.46
5	122	10.63	4.96	4.22
1-5, aggregated	38	14.98	7.43	6.72
1-5, aggregated	52	26.13	11.47	9.90
1-5, aggregated	66	33.80	13.57	11.57
1-5, aggregated	80	30.52	11.56	9.62
1-5, aggregated	94	22.64	8.27	6.90
1-5, aggregated	108	19.25	6.68	5.16
1-5, aggregated	122	12.65	4.23	3.41

Table A.3
Error metrics for predicting intermediate push forces with 3 grid curves.

Subject	Push Force in N	RMSE in Ns/M	RRMSE in %	MAPE in %
1	32	21.78	7.27	6.04
1	43	9.31	3.17	3.12
1	54	18.98	6.56	5.37
1	76	8.13	2.56	2.38
1	87	16.30	5.31	4.82
1	98	11.29	3.49	3.02
2	32	20.20	10.17	7.45
2	43	5.78	3.09	2.43
2	54	12.72	6.35	5.09
2	76	15.94	7.59	6.29
2	87	12.56	5.91	4.63
2	98	10.58	4.92	3.89
3	32	8.55	3.19	2.55
3	43	7.37	2.65	2.28
3	54	12.99	4.55	3.32
3	76	11.30	3.63	2.76
3	87	13.10	4.18	2.50
3	98	19.95	6.30	3.30
4	32	8.98	3.57	2.72
4	43	9.32	3.63	2.80
4	54	16.76	6.04	3.90
4	76	7.41	2.65	1.93
4	87	10.93	3.71	2.85
4	98	11.94	4.10	3.07
5	32	9.47	5.54	4.65
5	43	11.73	6.60	4.83
5	54	6.95	3.68	3.17
5	76	14.02	7.38	4.65
5	87	20.32	10.77	7.16
5	98	15.07	7.54	5.11
1-5, aggregated	32	11.93	5.34	4.04
1-5, aggregated	43	6.61	2.95	2.47
1-5, aggregated	54	6.13	2.66	2.16
1-5, aggregated	76	10.62	4.37	3.58
1-5, aggregated	87	10.78	4.37	3.35
1-5, aggregated	98	6.88	2.73	2.30

Table A.4
Error metrics for predicting intermediate grip forces with 3 grid curves.

Subject	Grip Force in N	RMSE in Ns/M	RRMSE in %	MAPE in %
1	38	11.14	4.67	4.11
1	52	11.27	4.34	4.40
1	66	14.88	5.05	4.73
1	94	14.19	4.14	3.61
1	108	9.56	2.68	2.29
1	122	7.50	2.06	1.92
2	38	9.08	5.46	4.88
2	52	7.84	4.38	3.34
2	66	8.31	4.20	3.53
2	94	8.10	3.60	2.59
2	108	7.24	3.04	2.76
2	122	17.32	6.85	5.60
3	38	18.22	7.60	6.59
3	52	16.68	6.41	5.32
3	66	14.01	4.99	3.77
3	94	22.06	6.84	3.74
3	108	10.89	3.30	2.22
3	122	9.18	2.71	1.75
4	38	8.85	4.05	3.48
4	52	10.71	4.46	4.01
4	66	10.09	3.81	3.22
4	94	7.01	2.43	1.94
4	108	7.85	2.59	2.09
4	122	5.33	1.70	1.22
5	38	9.66	6.86	4.67
5	52	16.00	9.30	8.22
5	66	12.83	7.17	5.98
5	94	10.91	5.40	4.20
5	108	8.83	4.33	3.18
5	122	7.74	3.61	2.82
1-5, aggregated	38	9.12	4.52	4.05
1-5, aggregated	52	12.17	5.34	4.75
1-5, aggregated	66	12.24	4.91	4.49
1-5, aggregated	94	8.31	3.04	2.31
1-5, aggregated	108	7.75	2.69	1.99
1-5, aggregated	122	6.88	2.30	1.86

Table A.5
Error metrics for predicting intermediate push forces with 4 grid curves.

Subject	Push Force in N	RMSE in Ns/M	RRMSE in %	MAPE in %
1	32	26.47	8.84	6.70
1	43	12.29	4.19	4.17
1	65	12.14	3.89	3.13
1	87	17.20	5.60	4.65
1	98	10.86	3.36	2.89
2	32	16.90	8.51	6.25
2	43	10.84	5.79	4.68
2	65	14.77	7.48	6.14
2	87	9.48	4.46	3.18
2	98	8.67	4.03	2.85
3	32	6.01	2.25	1.87
3	43	7.81	2.81	2.30
3	65	10.01	3.35	2.25
3	87	10.71	3.42	2.35
3	98	18.34	5.79	3.04
4	32	9.29	3.69	2.78
4	43	16.10	6.28	4.48
4	65	9.14	3.34	2.28
4	87	10.96	3.73	2.88
4	98	11.50	3.95	2.99
5	32	10.31	6.04	5.37
5	43	12.19	6.86	4.31
5	65	10.85	5.67	3.96
5	87	13.24	7.02	4.85
5	98	12.59	6.30	4.55
1-5, aggregated	32	11.04	4.94	3.81
1-5, aggregated	43	5.47	2.44	1.83
1-5, aggregated	65	7.13	3.00	2.53
1-5, aggregated	87	8.02	3.25	2.38
1-5, aggregated	98	4.99	1.98	1.58

Table A.6
Error metrics for predicting intermediate grip forces with 4 grid curves.

Subject	Grip Force in N	RMSE in Ns/M	RRMSE in	MAPE
1	38	8.45	3.54	2.68
1	52	10.06	3.87	3.54
1	80	9.87	3.16	3.02
1	108	5.11	1.43	1.19
1	122	9.98	2.74	2.44
2	38	8.98	5.40	4.73
2	52	6.55	3.66	2.61
2	80	10.04	4.58	3.62
2	108	7.82	3.28	2.69
2	122	17.33	6.85	5.57
3	38	14.68	6.12	5.36
3	52	10.68	4.11	3.49
3	80	10.34	3.40	2.88
3	108	13.54	4.11	2.67
3	122	10.66	3.14	2.04
4	38	8.52	3.90	3.25
4	52	8.35	3.48	2.90
4	80	7.46	2.68	2.14
4	108	6.94	2.29	1.79
4	122	5.11	1.64	1.16
5	38	8.36	5.94	4.64
5	52	11.93	6.94	5.88
5	80	8.19	4.33	3.56
5	108	9.46	4.64	3.39
5	122	6.63	3.10	2.53
1-5, aggregated	38	6.52	3.23	2.91
1-5, aggregated	52	6.09	2.67	2.33
1-5, aggregated	80	6.13	2.32	1.88
1-5, aggregated	108	6.56	2.28	1.76
1-5, aggregated	122	6.38	2.13	1.79